Generalized Adsorption Isotherms for Molecular and Dissociative Adsorption of a Polar Molecular Species on Two Polar Surface Geometries: Perovskite (100) (Pm-3m) and Fluorite (111) (Fm-3m)

Thomas Danielson[1], Celine Hin[1,2], Aditya Savara[3*]
*Corresponding Author: savaraa@ornl.gov
[1]*Department of Materials Science and Engineering, Virginia Polytechnic Institute and State University, Blacksburg, VA, USA*
[2]*Department of Mechanical Engineering, Virginia Polytechnic Institute and State University, Blacksburg, VA, USA*
[3]*Chemical Sciences Division, Oak Ridge National Laboratory, Oak Ridge, TN, USA*

Abstract

Lattice based kinetic Monte Carlo (KMC) simulations have been used to determine a functional form for the second order adsorption isotherms on two commonly investigated crystal surfaces: the (111) fluorite surface and the (100) perovskite surface which has the same geometric symmetry as the NaCl (100) surface. The functional form is generalized to be applicable to all values of the equilibrium constant by a shift along the pressure axis. Functions have been determined for estimating the pressure at which a desired coverage would be achieved and for estimating the coverage at a certain pressure. The generalized form has been calculated by investigating the surface adsorbate coverage across a range of thermodynamic equilibrium constants that span the range 10^{-26} to 10^{13}. The equations have been shown to be general for any value of the adsorption equilibrium constant.

Keywords: Molecular Adsorption, Dissociative Adsorption, Adsorption Isotherm, Perovskite, Fluorite

I. Introduction

Adsorption isotherms are functions which relate the coverage, θ, to the pressure, P, or other measure of the adsorbate's activity at a given pressure. Prior to the 20th century, adsorption isotherms were only obtainable via empirical data. The first analytical approximations for adsorption isotherms were developed by Langmuir in the early 20th century, but the underlying assumptions such as an adsorbate species that behaves like an ideal gas, no lateral interactions of adsorbates and a simple first order adsorption process, are valid for only the most elementary and controlled reactions [1]. Langmuir's approximations have been extended, in an analytical way, to include lateral interactions and higher order adsorption reaction processes [2-13], but currently, there are many adsorption processes and surface geometries which do not have an analytical solution, such as molecular adsorption of a polar molecule on a polar substrate. Thus, obtaining an adsorption isotherm for a particular gas adsorbing or reacting on a surface with a particular geometry would require experimentation or accurate simulation/modeling [14-22].

Lattice kinetic Monte Carlo (KMC) simulations are a tool for simulating chemical reactions on surfaces that can take into account the local configuration [23-27]. The probability of a particular reaction occurring in a given time period is based on the reaction rate, which is fixed by its rate constant and thus, the stochastic simulation technique is capable of mimicking the statistical occurrence of real-world reaction processes in a way that is exact, assuming that the model is accurately parameterized. As a result, performing lattice KMC simulations with adsorption and desorption processes allows an effective empirical method for determining adsorption isotherms with increased accuracy when compared to analytical approximations.

There is one historical case that is similar to the current study. Roberts and Miller [28] were able to derive an analytical form based on the Bethe approximation for dissociative adsorption of a dimer on a square lattice surface (such as H_2 or O_2 on a metal surface). Roberts and others [29, 30] also performed Monte Carlo simulations to derive an isotherm, and the analytical equation derived by Roberts and Miller deviated very strongly from the Monte Carlo simulations. Vette and others later [30, 31]used similar arguments to derive a more accurate expression that matched the Monte Carlo simulations very well. Monte Carlo simulations have also been performed in order to investigate dimer adsorption on substrates with varying geometries and energetic landscapes [32-34]. However, to the authors' knowledge, no studies on related isotherms for adsorption processes with orientation dependent behavior have been previously published (i.e., dissociation of molecules where the two halves are not equivalent and the two corresponding adsorption sites do not have competitive adsorption between them). In the current work, lattice KMC simulations have been used to determine a functional form for the adsorption isotherm across the entire parameter space on two different surface geometries of widespread interest; the (111) fluorite surface and the (100) perovskite surface. The isotherms for the (100) perovskite surface also apply to (100) surfaces for the NaCl structure, as these have the same geometric symmetry. For each surface, the general functional forms derived are capable of being used to determine the coverage as a function of pressure, or vice-a-versa, for any value of the equilibrium constant, and thus at any pressure. The same packing (and thus isotherms) should apply for cases of liquid to surface adsorption, as well.

II. Theoretical Background and Computational Setup

A. Theoretical Background for Analytical Solutions and KMC of Adsorption Isotherms

To understand the relationship between all adsorption isotherms for a given surface geometry, we first consider the analytical solution for an adsorption isotherm based on the Langmuir adsorption model (this is unrelated to how the kinetic Monte Carlo simulations are performed). First we define an adsorption process of a polar molecular species, *M*, on a polar substrate (i.e. a surface with two unequal sites, *A* and *B*, where the adsorption process results in a bridging occupation of both *A* and an adjacent *B*):

$$\mathbf{M}\ (g) + A + B_{adjacent} \rightarrow A - \mathbf{M}_{bridging}\ (ads) - B$$

or for a dissociative adsorption process:

$$\mathbf{M}\,(g) + A + B_{adjacent} \rightarrow \mathbf{M}^{+}\!-A + \mathbf{M}^{-}\!-B$$

In these types of adsorption processes, multiple molecular orientations are possible between *A* and *B* sites (during adsorption, an *A* site is filled along with only one of the *N* neighboring *B*). In the mean field approximation where local configurations are ignored, the rates of adsorption and desorption are proportional to the concentrations of the sites and surface species involved, allowing us to write:

$$r_{ads} = k_{ads}\, P[A][B] \quad (1)$$
$$r_{des} = k_{des}\ \theta \quad (2)$$

where *P* is the pressure, θ is the relative surface coverage, [A] is the fraction of open A sites, and [B] is the fraction of open B sites. The concentrations of the open sites and the surface coverage ([A], [B], θ) are each bound by [0,1]. k_{ads} and k_{des} are the rate constants for adsorption and desorption and are defined as:

$$k_{ads} = \frac{S_0}{\sqrt{2\pi k_B T m}} e^{\frac{-E_a}{RT}} \mathcal{A}_U \quad (3)$$
$$k_{des} = \alpha e^{\frac{-E_d}{RT}} \quad (4)$$

where S_0 is the steric factor from collision theory (see page 221 of reference [35]), k_B is the Boltzmann constant, *T* is the temperature, *m* is the molecular mass of the gas phase molecule, E_a is the activation energy, $\mathcal{A}_U$ is the area corresponding to an A site along with one adjacent B site, *R* is the gas constant and α is the pre-exponential factor (typically with units of s^{-1}).

When considering the impacts of local configurations, analytical solutions to the isotherm for this situation can be derived for the low coverage cases. In this case, the adsorption rate requires having an open *B* site next to an open *A* site, and we can write:

$$r_{ads} = k_{ads}\, P[A]\, [B]_{adjacent} \quad (5)$$

where $[B]_{adjacent}$ reflects the probability of an open B site adjacent to an open A site. The expression for the desorption rate does not include site concentrations and remains unchanged. Note that $[B] \neq [B]_{adjacent}$: The former is the global concentration of B, while the latter is the concentration of B directly adjacent to a particular A site.

At very low coverages (e.g. $\theta \leq 0.01$), we can say that to a very good approximation any unoccupied *A* is neighboring an unoccupied *B*. Thus, the rate of adsorption can be simplified based on the approximation that all *B* sites are unoccupied (i.e. $[B]_{adjacent} = 1$) which gives:

$$r_{ads} = k_{ads}\, P[A]\, [B]_{adjacent} = k_{ads}\, P[A] = k_{ads}\, P\, (1 - \theta) \quad (6)$$

At equilibrium, the forward and reverse rates are equal, so we can set the forward and reverse rates equal followed by rearranging to obtain an expression for the isotherm. Using eq. 6 for the rate of adsorption and eq 2 for the rate of desorption, setting $r_{ads} = r_{des}$, we find that the very low coverage isotherm can be approximated by:

$$\theta_i = \frac{KP}{1 + KP} \; where \; K_i = \frac{k_{ads}}{k_{des}} \quad (7)$$

where K is the equilibrium rate constant of adsorption and desorption for a specific isotherm (i.e., specific temperature and surface), and K has units of inverse pressure.

For medium coverages (e.g. $0.1 \leq \theta \leq 0.3$), the approximation that all *B* sites are uncovered no longer holds. Instead, the odds of finding an unoccupied *B* site adjacent to an unoccupied *A* site is approximately the same as the odds of finding an unoccupied *A* site to begin with (i.e. $[B]_{adjacent} \approx [A]$). Using this approximation, the rates of adsorption and desorption are defined as:

$$r_{ads} = k_{ads}\, P[A]\, [B]_{adjacent} = k_{ads}\, P[A][A] = k_{ads}\, P\, (1 - \theta)^2 \quad (8)$$

$$r_{des} = k_{des}\ \theta \quad (9)$$

and again, setting $r_{ads} = r_{des}$, the equilibrium coverage for a given isotherm is:

$$\theta_i = \frac{2KP - \sqrt{4KP + 1} + 1}{2KP} \quad (10)$$

At high coverages (e.g. $\theta \geq 0.3$), we can no longer analytically determine the surface concentration of *B* sites because it is uncertain how increasing the occupation of *A* sites affects the concentration of *B* sites adjacent to unoccupied *A* sites. Thus, a numerical method, such as KMC, is necessary in order to determine the equilibrium coverage for the high coverage regimes.

Lattice kinetic Monte Carlo simulations within the KMOS framework [36] have been used to determine a functional form for all coverage regimes of the adsorption isotherm of a polar adsorption process. Within the lattice KMC framework, the surface stochastically evolves through time along a trajectory of configuration space that is probabilistically defined by the transition frequencies, *w*, for the processes considered. While KMC is often utilized to investigate the time evolution of a kinetic system, the steady-state kinetics can be understood based on an average across simulation steps in which steady-state has been achieved. The KMC algorithm used for the current work uses the variable step size method, which is described in reference [36]. The simulations began with bare surfaces (no adsorbates) and were run for 10^6 KMC steps. For all KMC simulations, 10^6 KMC steps were more than sufficient to reach equilibrium, and the

equilibrium concentrations used to develop the functional forms were taken from the arithmetic average across the final 2 x 10^5 KMC steps.

The link between KMC and the analytical solutions for the equilibrium coverage of a specific adsorption isotherm is made by the fact that the probability of the system transitioning (i.e. transition frequency, *w*) from configuration *u* to a subsequent configuration *v* via reaction process *q* is defined by the same kinetic parameters (activation energy and pre-exponential) as the chemical kinetics reaction rate constant for that reaction. However, the probability of a reaction occurring within KMC is also defined by the surface configuration (as opposed to surface concentration in the analytical formulations). That is, if the surface configuration is such that process *q* can occur, the reaction process's transition frequency is *w*. If the configuration is such that process *q* cannot occur, the reaction process's transition frequency is 0 until a configuration arises where the process can occur. Thus, on a particular site, *s*, the rate at which a particular reaction, *q*, transitions the system to a new configuration is proportional to the number of times that the local configuration exists where process *q* is available to occur. That is:

$$r_q^s = w_q C_o \tag{11}$$

where C_o is 0 or 1, depending on whether or not the configuration exists. From this, the net rate of reaction *q* is:

$$r_q^{net} = \sum_1^N w_q C_o \tag{12}$$

where *N* is the total number of a particular site type on which reaction process *q* can occur.

If we define configuration *u* to be the surface with *N* adsorbates and configuration *v* to be the surface with *N-1* adsorbates, the reaction process, *q*, is desorption and *w* is defined by:

$$w_{des}^{u\to v} = \alpha e^{\frac{-E_d}{RT}} \tag{13}$$

Alternatively, if the initial configuration, *u*, is the surface with *N* adsorbates and configuration *v* is the surface with *N+1* adsorbates, the reaction process *q* is adsorption and *w* is defined by:

$$w_{ads}^{u\to v} = \frac{P * \mathcal{A}_C * S_0}{\sqrt{2\pi k_B T m}} e^{\frac{-E_a}{RT}} \tag{14}$$

where S_0 is the steric factor, *P* is the pressure and $\mathcal{A}_C$ is the area corresponding to the KMC cell for which the transition is being defined (which can be larger than a single site). In our simulations, $\mathcal{A}_C$ corresponds to a single KMC unit cell, which can be larger than one crystallographic primitive unit cell.

From this, the evolution of the surface concentration in a KMC simulation containing adsorption and desorption processes is given by:

$$\frac{d\theta}{dt} = r_{ads}^{net} - r_{des}^{net} \tag{15}$$

The equilibrium surface coverages depend upon the balance of the rates of adsorption and desorption, which in turn depend upon the adsorption and desorption transition frequencies (i.e. $W_{Eq} = \frac{w_{ads}}{w_{des}}$). To find a functional form that extends across the entire realistic parameter space for the ratio of w_{ads} to w_{des}, realistic upper and lower bounds of adsorption equilibrium constants were determined and KMC simulations covering equilibrium constants spanning the entire realistic parameter space have been investigated. Realistic ranges for the kinetic parameters are shown in Table I, and were used to determine realistic bounds for the equilibrium constant. Based on the boundaries in Table I, the lower and upper bounds for realistic thermodynamic equilibrium constants for gas-solid adsorption are 10^{-26} and 10^{13} respectively, with 1 bar as the reference pressure (P°). We do not include the reference states for the surface states explicitly, which implies that they cancel, in line with common practice for the thermodynamic analysis of adsorption on surfaces [37, 38]. The molecular mass of methanol (32 atomic mass units) was used in the adsorption rate constant: all phase molecules under standard conditions have masses within 1 order of magnitude of methanol, so the bounds here are broad and realistic. The isotherms obtained are applicable to all molecules.

TABLE I. Upper and lower bounds for all relevant parameters in k_{ads} and k_{des}

	Lower Bound	***Upper Bound***
$\boldsymbol{P}$	10^{-8} bar	10 bar
S_0	10^{-6}	1
$\boldsymbol{T}$	5 K	1000 K
$\boldsymbol{E_d}$	10 kJ/mol	200 kJ/mol
$\boldsymbol{E_a}$	0 kJ/mol	N/A
α	10^{9} s^{-1}	10^{18} s^{-1}

The adsorption isotherms for a polar molecule have been investigated on two distinct, multi-species surfaces: the fluorite (111) surface (e.g. CeO_2) and the perovskite (100) surface (e.g. $CaTiO_3$), shown in Figure 1. Below, we consider the sites corresponding to *A* and *B* in Equations 16 and 17 to be a cation and an anion, though the work is general enough to apply to other surfaces. Within this context, the adsorption process has been investigated for the situations of non-dissociative adsorption and dissociative adsorption in the absence of diffusion limitations:

1) Non-dissociative Adsorption (a.k.a. Molecular Adsorption) occurs where there is a bridging of a polar molecule between the two distinct surface species (e.g. molecular adsorption

of CH_3OH bridging between a cation and an anion with the CH_3O end occupying the cation site and the H end occupying the anion site), but no dissociation of the molecule occurs.

2) Dissociative adsorption occurs where immediately upon adsorption, the molecule dissociates (e.g. dissociative adsorption of CH_3OH that results in CH_3O^- occupying the cation site and the H^+ occupying the anion site).

The conditions that must be satisfied for the adsorption processes to occur are: an unoccupied cation site and at least one unoccupied first nearest neighbor anion site. As can be seen in Figure 1, this gives a maximum of three molecular orientations for each cation site on the fluorite (111) surface and four molecular orientations on the perovskite (100) surface. If more than one of the neighboring anion sites are unoccupied, the orientation of the adsorbate is randomly selected with an equal probability defined by the adsorption transition frequency. Within the KMC simulation of this study, the simulation size contains on the order of 400 unit cells and periodic boundary conditions are applied in the *x* and *y* directions, where this simulation size is large enough to provide sufficient KMC statistics and avoid simulation-size related artifacts. We have also performed simulations with 50 site pairs, and we have not observed differences between the two sizes. Additionally, if there were long-range finite size effects (such as ordering), these would appear as kinks in the isotherm -- as seen in the figures of this work, no such kinks were observed.

The surface unit cell for each structure investigated is indicated by the black box in Figure 1. There are two distinct anion sites and two distinct cation sites in each structure. Each orientation on each surface site has its own transition frequency, *w*, though in reality, the kinetics of each is defined by the same energetics. As a result of this, the net transition frequency for adsorption processes on each cation site is:

$$w_{Ads}^{net,Fluorite} = w_{ads}^{A-B1} + w_{ads}^{A-B2} + w_{ads}^{A-B3} \tag{16}$$

$$w_{Ads}^{net,Perovskite} = w_{ads}^{A-B1} + w_{ads}^{A-B2} + w_{ads}^{A-B3} + w_{ads}^{A-B4} \tag{17}$$

where w_{ads}^{A-B1} would indicate the transition frequency for an adsorption process to occur where the molecule is bridging (or dissociating) between the cation site, *A*, and the neighboring anion site, *B1*, as shown for each surface configuration in Figure 1. In a more generalized form, the net transition frequency of adsorption on a cation site that has multiple possible orientations between surrounding anion sites is given as:

$$w_{Ads}^{net} = \sum_{i=1}^{M} w_{ads}^{i} \tag{18}$$

where *M* is the number of possible orientations on all sites within the kinetic Monte Carlo simulation cell ($\mathcal{A}_C$), and w_{ads}^{i} is the adsorption rate constant for a specific A-B orientation, *i*. The rate constants from Eq. 2 and 3 are different from the transition frequencies in KMC, since the

former depends on concentrations and the latter depends on configurations. To understand the relationship between the chemical kinetics rate constant for adsorption and the KMC transition frequency for adsorption, we need to look at the *net rate* of adsorption. To compare the net rate of adsorption from KMC to the net rate of adsorption from the analytical solution for a given surface area, we must convert the relative rate from Eq. 6 to an absolute rate (i.e. $\frac{molecules}{m^2 s}$) by dividing Eq. 6 by area $\mathcal{A}_u$ and then multiplying by the area considered in the KMC simulation, $\mathcal{A}_C$. In doing so, comparing the absolute rates of adsorption from Eqs. 6 and 18 (for an area of $\mathcal{A}_C$):

$$\frac{k_{ads}\, P[A]}{\mathcal{A}_U}\mathcal{A}_C \;\; versus \sum_{i=1}^{M} w_{ads}^{i} C_o \tag{19}$$

For our simulations, $\mathcal{A}_C = 2\mathcal{A}_U$, because our KMC unit cells encompassed 2 cations and 2 anions. We can find a relationship between k_{ads} and w_{ads} with the use of a symmetry factor, X, that corresponds to the presence of equivalent configurations in the KMC that are not separated explicitly in the mean-field equations. For the case when $[A] = C_o$:

$$X(2k_{ads}\, P) = \sum_{i=1}^{M} w_{ads}^{i} \tag{20}$$

where X is the factor that accounts for the number of possible adsorption orientations in the area $\mathcal{A}_U$. In this case, the number of orientations comes from the symmetry, and we find that $X = 3$ for the fluorite (111) structure and $X=4$ for the perovskite (100) structure. In our simulations, the fluorite structure has 6 orientations in within a KMC unit cell ($\mathcal{A}_C = 2.534x10^{-19}\ m^2$), and the perovskite structure has 8 orientations within a KMC unit cell ($\mathcal{A}_C = 1.46x10^{-19}\ m^2$).

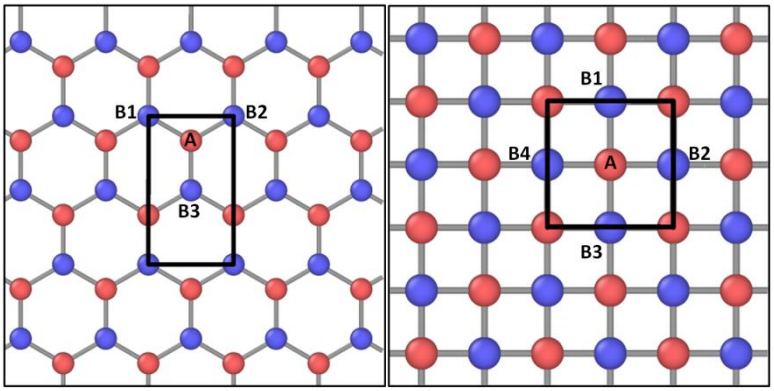

FIG. 1. (Left) Flourite (111) Structure and (Right) perovskite (100) structure. The black box indicates a single surface KMC unit cell. A and B labels indicate surface cation and anion sites respectively.

The surface coverage for the upper and lower bounds of the equilibrium transition frequency ratio was calculated across a range of pressures that corresponds to coverages in the

range of [0,1]. The calculated functional form is general for each surface geometry and each adsorption type and thus, the atomic surface species are less important than the geometry of the surface which defines the way in which the adsorption process occurs.

B. Generalization of the adsorption isotherms

The isotherms for low and medium coverages (Eqs. 7 and 10) can be extended to any value of the equilibrium constant based on a shift along the log(P) axis, since *K* appears as a coefficient of *P*. That is, to determine the coverage of a different isotherm, $\theta_2(P)$, where K_1 is related to K_2 by a constant, *c*, we have:

$$cK_1 = K_2 \tag{21}$$

$$\theta_2 = \frac{cK_1P}{1 + cK_1P} \tag{22}$$

Which can be rewritten as:

$$\theta_2 = \frac{10^{Log(cK_1)}10^{Log(P)}}{1 + 10^{Log(cK_1)}10^{Log(P)}} = \frac{10^{Log(K_1)+Log(P)+Log(c)}}{1 + 10^{Log(K_1)+Log(P)+Log(c)}} \tag{23}$$

This shows that when changing the equilibrium constant from K_1 to K_2, the isotherm has the same functional form, with the new coverage θ_2, shifted along the log(P) axis by a factor of *c*. The same can be shown for the medium coverage case from eq. 10. It is clear that the most important factor for determining any given isotherm is the equilibrium constant and also that a generalized functional form exists for all isotherms with respect to a given surface geometry, provided that K appears as a coefficient of P in the form of the isotherm that is solved for coverage. If the KMC derived isotherms also have this attribute (that K can be treated as a coefficient of P when the isotherm is solved for coverage) then the KMC derived isotherms will also be generalizable for arbitrary values of K.

III. Results

In the current section, we present functional forms for the adsorption isotherms for both the (111) fluorite and (100) perovskite surface geometries (with either the pressure or coverage being the dependent variable). The generalizability of the functional forms for any value of K will be shown. In all equations of this manuscript, "log" implies the logarithm with base 10. We use a factor of (P°/P°) to obtain unitless quantities for separation of the log terms, utilizing KP x (P°/P°) = (KP°) x (P/P°). The KMC simulations started with bare surfaces (no adsorbates) and were run until equilibrium was reached. The equilibrium coverages from the KMC simulations, which were used to obtain the functional forms for each of the adsorption isotherms, is provided in the supplemental material (available online) [39] Tables SI – SIV.

A. Perovskite (100) surface geometry

1. Non-Dissociative Adsorption (Molecular Adsorption)

To obtain an isotherm functional form for molecular adsorption on the (100) perovskite surface geometry, 100 different pressures in the range 0.0014 to 1606525 bar were applied to an adsorption isotherm with KP° = 0.018001. This corresponds to 100 KMC simulations which were used to calculate the steady-state surface coverage at each pressure. The functional dependence of the coverage on the log of pressure for the adsorption isotherm is described by piecewise fitting applied to two regions (fit to KMC data shown in Figure 2):

$$\boldsymbol{For\ Log\left(\frac{P}{P^{\circ}}\right) \epsilon\ [-2.8551, 1.4035]},$$

$$\begin{aligned}\theta = {} & 0.118366 + 0.225402\left(Log\left(\frac{P}{P^{\circ}}\right) - Log\left(\frac{KP^{\circ}}{0.072004}\right)\right) \\ & + 0.140317\left(Log\left(\frac{P}{P^{\circ}}\right) - Log\left(\frac{KP^{\circ}}{0.072004}\right)\right)^{2} \\ & + 0.00648402\left(Log\left(\frac{P}{P^{\circ}}\right) - Log\left(\frac{KP^{\circ}}{0.072004}\right)\right)^{3} \\ & - 0.0198329\left(Log\left(\frac{P}{P^{\circ}}\right) - Log\left(\frac{KP^{\circ}}{0.072004}\right)\right)^{4} \\ & - 0.0045132\left(Log\left(\frac{P}{P^{\circ}}\right) - Log\left(\frac{KP^{\circ}}{0.072004}\right)\right)^{5}\end{aligned} \tag{24}$$

$$\boldsymbol{For\ Log\left(\frac{P}{P^{\circ}}\right) \epsilon\ [1.4035, 6.205887]},$$

$$\begin{aligned}\theta = {} & -0.270651 + 0.981059\left(Log\left(\frac{P}{P^{\circ}}\right) - Log\left(\frac{KP^{\circ}}{0.072004}\right)\right) \\ & - 0.30278\left(Log\left(\frac{P}{P^{\circ}}\right) - Log\left(\frac{KP^{\circ}}{0.072004}\right)\right)^{2} \\ & + 0.0457836\left(Log\left(\frac{P}{P^{\circ}}\right) - Log\left(\frac{KP^{\circ}}{0.072004}\right)\right)^{3} \\ & - 0.00330246\left(Log\left(\frac{P}{P^{\circ}}\right) - Log\left(\frac{KP^{\circ}}{0.072004}\right)\right)^{4} \\ & + 0.0000865719\left(Log\left(\frac{P}{P^{\circ}}\right) - Log\left(\frac{KP^{\circ}}{0.072004}\right)\right)^{5}\end{aligned} \tag{25}$$

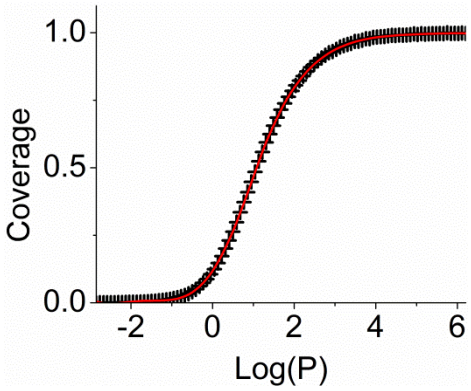

FIG. 2. Functional (red line) dependence of coverage on pressure from KMC simulations (black symbols) of molecular adsorption on the perovskite (100) surface, fitted with a piecewise function.

The inverse function, which is the functional dependence of the log of pressure on the coverage is described using piecewise fitting applied to four regions as follows functions (fit to KMC data in Figure 3):

$$\boldsymbol{For\ \theta\ \epsilon\ [0.00025, 0.124625]},\quad \boldsymbol{Log\left(\frac{P}{P^{\circ}}\right) = \left(0.944439 + 0.463005 * Ln(\theta)\right) - Log\left(\frac{KP^{\circ}}{0.072004}\right)} \tag{26}$$

$$\boldsymbol{For\ \theta\ \epsilon\ [0.12645, 0.87175]},\quad \boldsymbol{Log\left(\frac{P}{P^{\circ}}\right) = (-0.612019 + 6.00428\theta - 8.36136\theta^{2} + 6.21532\theta^{3}) - Log\left(\frac{KP^{\circ}}{0.072004}\right)} \tag{27}$$

$$\boldsymbol{For\ \theta\ \epsilon\ [0.87175, 0.991]},\quad \boldsymbol{Log\left(\frac{P}{P^{\circ}}\right) = (-580.433 + 2001.12\theta - 2294.26\theta^{2} + 878.394\theta^{3}) - Log\left(\frac{KP^{\circ}}{0.072004}\right)} \tag{28}$$

$$\boldsymbol{For\ \theta\ \epsilon\ [0.991, 0.99725]},\quad \boldsymbol{Log\left(\frac{P}{P^{\circ}}\right) = (-114767 + 353107\theta - 362150\theta^{2} + 123816\theta^{3}) - Log\left(\frac{KP^{\circ}}{0.072004}\right)} \tag{29}$$

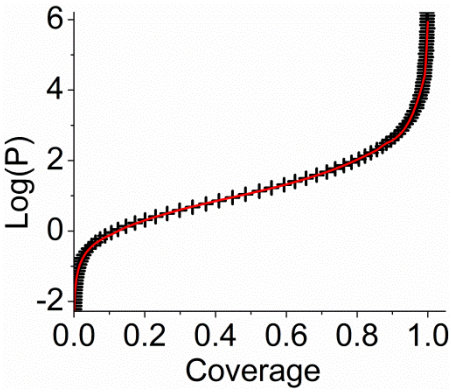

FIG. 3. Functional dependence (red line) of pressure on coverage from KMC simulations (black symbols) of molecular adsorption on the perovskite (100) surface, fitted with a piecewise function.

In order to illustrate the generalizability of the adsorption isotherm across an entire parameter space of equilibrium rate constants, multiple adsorption isotherms have been simulated and the shift along the log(P) axis has been investigated. Figure 4 shows that the adsorption isotherms are shifted along the pressure axis by a factor of $c = Log(\frac{W_2}{W_1})$. The central line is the generalized fit to the original isotherm and the curves on the left and right are the lower and upper bound with the shifted fit functional form. The markers indicate the actual output of the adsorption isotherm from the KMC simulation.

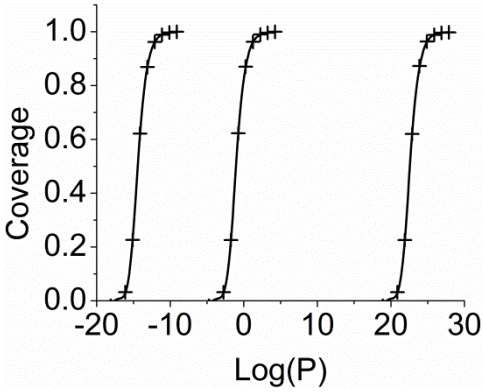

FIG. 4. Illustration of the generalization of the functional form for any isotherm between the upper and lower bounds. The central data set corresponds to the location along the log(P) axis of the original fit and the markers are the KMC data. The data sets to the left and right of the central data set are the extremes close to the upper bound ($KP° = 1.656x10^{12}$) and lower bound ($KP° = 1.656x10^{-25}$) of the equilbrium parameter space. The data is plotted with the piece-wise function from Eqs 24 and 25. As can be seen, this single piecewise function matches all of the KMC simulations.

2. Dissociative Adsorption

Dissociative adsorption was investigated across the same range of pressures for the same value of K. The functional dependence of coverage on the log of pressure is described by piecewise fitting applied to two regions as follows (fit to KMC data shown in Figure 5):

$$\boldsymbol{For\ Log\left(\frac{P}{P^{\circ}}\right) \epsilon\ [-2.8551833, 1.13169]},$$

$$\begin{aligned}\theta = {} & 0.161556 + 0.158883\left(Log\left(\frac{P}{P^{\circ}}\right) - Log\left(\frac{KP^{\circ}}{0.072004}\right)\right) \\ & + 0.0604624\left(Log\left(\frac{P}{P^{\circ}}\right) - Log\left(\frac{KP^{\circ}}{0.072004}\right)\right)^{2} \\ & + 0.00448308\left(Log\left(\frac{P}{P^{\circ}}\right) - Log\left(\frac{KP^{\circ}}{0.072004}\right)\right)^{3} \\ & - 0.0033256\left(Log\left(\frac{P}{P^{\circ}}\right) - Log\left(\frac{KP^{\circ}}{0.072004}\right)\right)^{4} \\ & - 0.0007052\left(Log\left(\frac{P}{P^{\circ}}\right) - Log\left(\frac{KP^{\circ}}{0.072004}\right)\right)^{5}\end{aligned} \tag{30}$$

$$\boldsymbol{For\ Log\left(\frac{P}{P^{\circ}}\right)\ \epsilon\ [1.13169, 6.205887]},$$

$$\begin{aligned}\boldsymbol{\theta} = \mathbf{0.173997} &+ \mathbf{0.0544927}\left(\boldsymbol{Log\left(\frac{P}{P^{\circ}}\right) - Log\left(\frac{KP^{\circ}}{0.072004}\right)}\right) \\ &+ \mathbf{0.224246}\left(\boldsymbol{Log\left(\frac{P}{P^{\circ}}\right) - Log\left(\frac{KP^{\circ}}{0.072004}\right)}\right)^{\mathbf{2}} \\ &- \mathbf{0.0866211}\left(\boldsymbol{Log\left(\frac{P}{P^{\circ}}\right) - Log\left(\frac{KP^{\circ}}{0.072004}\right)}\right)^{\mathbf{3}} \\ &+ \mathbf{0.0123429}\left(\boldsymbol{Log\left(\frac{P}{P^{\circ}}\right) - Log\left(\frac{KP^{\circ}}{0.072004}\right)}\right)^{\mathbf{4}} \\ &- \mathbf{0.0006257}\left(\boldsymbol{Log\left(\frac{P}{P^{\circ}}\right) - Log\left(\frac{KP^{\circ}}{0.072004}\right)}\right)^{\mathbf{5}}\end{aligned} \tag{31}$$

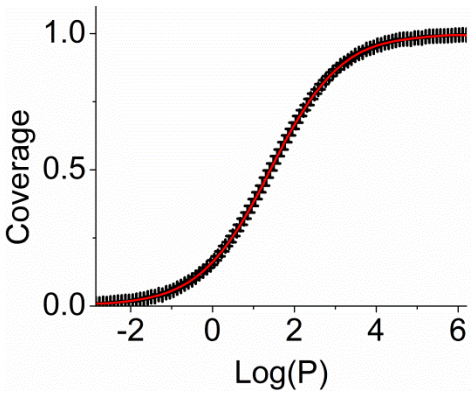

FIG. 5. Functional dependence (red line) of coverage on pressure from KMC simulations (black symbols) of dissociative adsorption on the perovskite (100) surface, fitted with a piecewise function.

The functional dependence of the log of pressure on the coverage can be described using piecewise fitting applied to four regions as follows (fit to KMC data shown in Figure 6):

$$\boldsymbol{For\ \theta\ \epsilon\ [0.009625, 0.0725625]},$$

$$\boldsymbol{Log\left(\frac{P}{P^{\circ}}\right) = \left(1.74793 + 0.950838 * Ln(\theta)\right) - Log\left(\frac{KP^{\circ}}{0.072004}\right)} \tag{32}$$

$$\boldsymbol{For\ \theta\ \epsilon\ [0.0725625, 0.81425]},$$

$$\begin{aligned}\boldsymbol{Log\left(\frac{P}{P^{\circ}}\right)} &= \left(-\mathbf{1.40205} + \mathbf{10.6793}\boldsymbol{\theta} - \mathbf{15.2563}\boldsymbol{\theta^{2}} + \mathbf{10.3187}\boldsymbol{\theta^{3}}\right) \\ &\quad - \boldsymbol{Log\left(\frac{KP^{\circ}}{0.072004}\right)}\end{aligned} \tag{33}$$

$$\textbf{For } \boldsymbol{\theta} \in [\mathbf{0.81425}, \mathbf{0.98431}], \tag{34}$$

$$\boldsymbol{Log}\left(\frac{\boldsymbol{P}}{\boldsymbol{P^{\circ}}}\right) = \left(-\mathbf{274.236} + \mathbf{974.356}\boldsymbol{\theta} - \mathbf{1147.74}\boldsymbol{\theta^2} + \mathbf{452.991}\boldsymbol{\theta^3}\right) - \boldsymbol{Log}\left(\frac{\boldsymbol{KP^{\circ}}}{0.072004}\right)$$

$$\textbf{For } \boldsymbol{\theta} \in [\mathbf{0.98431}, \mathbf{0.994875}], \tag{35}$$

$$\boldsymbol{Log}\left(\frac{\boldsymbol{P}}{\boldsymbol{P^{\circ}}}\right) = \left(-\mathbf{13170.2} + \mathbf{44305.60}\boldsymbol{\theta} - \mathbf{49280.5}\boldsymbol{\theta^2} + \mathbf{18152}\boldsymbol{\theta^3}\right) - \boldsymbol{Log}\left(\frac{\boldsymbol{KP^{\circ}}}{0.072004}\right)$$

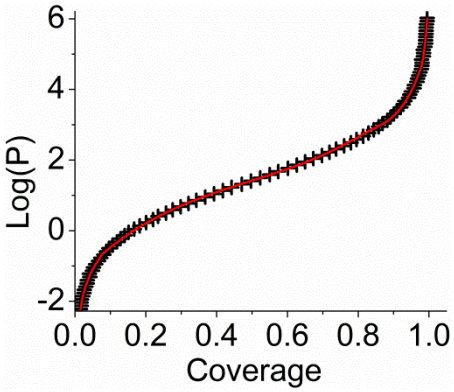

FIG. 6. Functional dependence (red line) of pressure on coverage from KMC simulations (black symbols) of dissociative adsorption on the perovskite (100) surface, fitted with a piecewise function.

In the dissociative case, the horizontal shift again reproduces the adsorption isotherms across the entire parameter space K in a similar fashion to the molecular adsorption case.

B. Fluorite (111) surface geometry

1. Molecular Adsorption

To obtain a functional form for molecular adsorption on the (111) fluorite surface geometry, 100 KMC simulations were run with pressures in the range 1.1×10^{-9} to 1.262 (bar) with KP° = 916313.5. The functional dependence of coverage on the log of pressure for this isotherm is described by piecewise fitting applied to two regions as follows (fit to KMC data shown in Figure 7):

$$\textbf{For } \boldsymbol{Log}\left(\frac{\boldsymbol{P}}{\boldsymbol{P^{\circ}}}\right) \in [-\mathbf{8.9599}, -\mathbf{5.60727}], \tag{36}$$

$$\boldsymbol{\theta = -187.408 - 130.695\left(Log\left(\frac{P}{P^{\circ}}\right) - Log\left(\frac{KP^{\circ}}{916313.5}\right)\right)}$$
$$\boldsymbol{- 35.6458\left(Log\left(\frac{P}{P^{\circ}}\right) - Log\left(\frac{KP^{\circ}}{916313.5}\right)\right)^{2}}$$
$$\boldsymbol{- 4.78022\left(Log\left(\frac{P}{P^{\circ}}\right) - Log\left(\frac{KP^{\circ}}{916313.5}\right)\right)^{3}}$$
$$\boldsymbol{- 0.316384\left(Log\left(\frac{P}{P^{\circ}}\right) - Log\left(\frac{KP^{\circ}}{916313.5}\right)\right)^{4}}$$
$$\boldsymbol{- 0.0082893\left(Log\left(\frac{P}{P^{\circ}}\right) - Log\left(\frac{KP^{\circ}}{916313.5}\right)\right)^{5}}$$

$$\boldsymbol{For\ Log\left(\frac{P}{P^{\circ}}\right) \epsilon\ [-5.6073, 0.101203],} \tag{37}$$

$$\boldsymbol{\theta = 0.999419 - 0.0004015\left(Log\left(\frac{P}{P^{\circ}}\right) - Log\left(\frac{KP^{\circ}}{916313.5}\right)\right)}$$
$$\boldsymbol{- 0.0029524\left(Log\left(\frac{P}{P^{\circ}}\right) - Log\left(\frac{KP^{\circ}}{916313.5}\right)\right)^{2}}$$
$$\boldsymbol{- 0.0008746\left(Log\left(\frac{P}{P^{\circ}}\right) - Log\left(\frac{KP^{\circ}}{916313.5}\right)\right)^{3}}$$
$$\boldsymbol{+ 9.7722x10^{-5}\left(Log\left(\frac{P}{P^{\circ}}\right) - Log\left(\frac{KP^{\circ}}{916313.5}\right)\right)^{4}}$$
$$\boldsymbol{+ 9.6801x10^{-5}\left(Log\left(\frac{P}{P^{\circ}}\right) - Log\left(\frac{KP^{\circ}}{916313.5}\right)\right)^{5}}$$

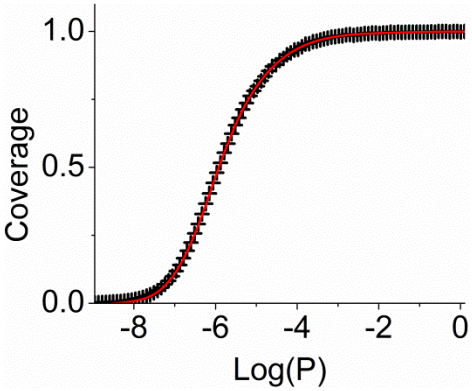

FIG. 7. Functional dependence (red line) of coverage on pressure from KMC simulations (black symbols) of molecular adsorption on the fluorite (111) surface, fitted with a piecewise function.

The functional dependence of the log of pressure on the coverage for a particular isotherm is described using piecewise fitting applied to four regions as follows (fit to KMC data shown in Figure 8):

$$\boldsymbol{For\ \theta\ \epsilon\ [0.002125, 0.05725],} \tag{38}$$
$$\boldsymbol{Log\left(\frac{P}{P^{\circ}}\right) = \left(-5.88671 + 0.495858 * Ln(\theta)\right) - Log\left(\frac{KP^{\circ}}{916313.5}\right)}$$

$$\boldsymbol{For\ \theta\ \epsilon\ [0.05725, 0.7985]},\qquad (39)$$

$$\boldsymbol{Log}\left(\frac{\boldsymbol{P}}{\boldsymbol{P^{\circ}}}\right) = (\boldsymbol{-7.60375 + 6.08201\theta - 8.69927\theta^{2} + 6.5102\theta^{3}}) - \boldsymbol{Log}\left(\frac{\boldsymbol{KP^{\circ}}}{916313.5}\right)$$

$$\boldsymbol{For\ \theta\ \epsilon\ [0.7985, 0.97225]},\qquad (40)$$

$$\boldsymbol{Log}\left(\frac{\boldsymbol{P}}{\boldsymbol{P^{\circ}}}\right) = (\boldsymbol{-112.983 + 386.32\theta - 465.93\theta^{2} + 189.752\theta^{3}}) - \boldsymbol{Log}\left(\frac{\boldsymbol{KP^{\circ}}}{916313.5}\right)$$

$$\boldsymbol{For\ \theta\ \epsilon\ [0.97225, 0.992]},\qquad (41)$$

$$\boldsymbol{Log}\left(\frac{\boldsymbol{P}}{\boldsymbol{P^{\circ}}}\right) = (\boldsymbol{7564.51 - 22141.6\theta + 21499.9\theta^{2} - 6924.54\theta^{3}}) - \boldsymbol{Log}\left(\frac{\boldsymbol{KP^{\circ}}}{916313.5}\right)$$

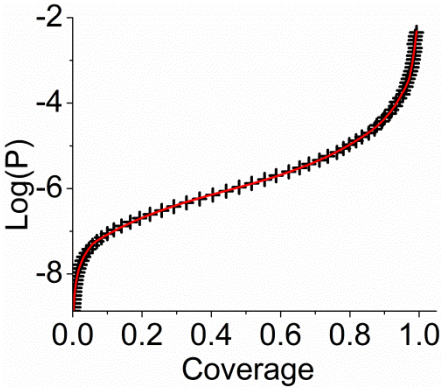

FIG. 8. Functional dependence (red line) of pressure on coverage from KMC simulations (black symbols) of molecular adsorption on the fluorite (111) surface, fitted with a piecewise function.

Once again, the functional form is shifted along the log(P) axis and shows that a different surface geometry does not affect the ability of the function to represent the entire parameter space in a general form.

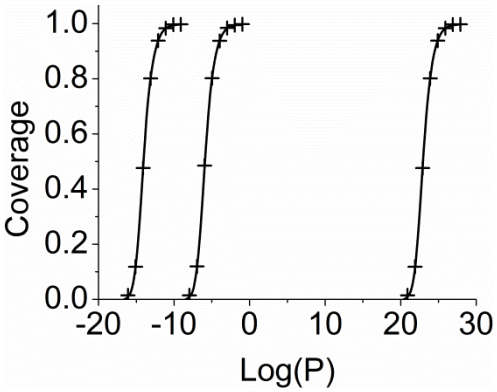

FIG. 9. Illustration of the generalization of the functional form for any isotherm between the upper and lower bounds. The central data set corresponds to the location along the log(P) axis of the original fit and the markers are the KMC data. The data sets to the left and right of the central data set are the etremes close to the upper bound ($KP^\circ = 1.248\text{x}10^{14}$) and lower bound ($KP^\circ = 1.248\text{x}10^{-23}$) of the equilbrium parameter space. The data is plotted with the piece-wise function from Eqs 36 and 27. As can be seen, this single piecewise function matches all of the KMC simulations.

2. Dissociative Adsorption

The generalized functional form of the adsorption isotherm for dissociative adsorption on the Fluorite (111) surface geometry has been investigated for the same adsorption isotherm as the molecular adsorption case. The functional dependence of coverage on the log of pressure for isotherm is described by piecewise fitting applied to two regions as follows (fit to KMC data shown in Figure 10):

$$\boldsymbol{For\ Log}\left(\frac{\boldsymbol{P}}{\boldsymbol{P^\circ}}\right)\boldsymbol{\epsilon}\ [\boldsymbol{-8.9599, -5.15422}], \tag{42}$$

$$\begin{aligned}\boldsymbol{\theta} = \boldsymbol{-19.5558} &\boldsymbol{- 14.6236}\left(\boldsymbol{Log}\left(\frac{\boldsymbol{P}}{\boldsymbol{P^\circ}}\right) - \boldsymbol{Log}\left(\frac{\boldsymbol{KP^\circ}}{916313.5}\right)\right)\\ &\boldsymbol{- 3.98238}\left(\boldsymbol{Log}\left(\frac{\boldsymbol{P}}{\boldsymbol{P^\circ}}\right) - \boldsymbol{Log}\left(\frac{\boldsymbol{KP^\circ}}{916313.5}\right)\right)^{\boldsymbol{2}}\\ &\boldsymbol{- 0.514522}\left(\boldsymbol{Log}\left(\frac{\boldsymbol{P}}{\boldsymbol{P^\circ}}\right) - \boldsymbol{Log}\left(\frac{\boldsymbol{KP^\circ}}{916313.5}\right)\right)^{\boldsymbol{3}}\\ &\boldsymbol{- 0.032126}\left(\boldsymbol{Log}\left(\frac{\boldsymbol{P}}{\boldsymbol{P^\circ}}\right) - \boldsymbol{Log}\left(\frac{\boldsymbol{KP^\circ}}{916313.5}\right)\right)^{\boldsymbol{4}}\\ &\boldsymbol{- 0.000782926}\left(\boldsymbol{Log}\left(\frac{\boldsymbol{P}}{\boldsymbol{P^\circ}}\right) - \boldsymbol{Log}\left(\frac{\boldsymbol{KP^\circ}}{916313.5}\right)\right)^{\boldsymbol{5}}\end{aligned}$$

$$\boldsymbol{For\ Log\left(\frac{P}{P^{\circ}}\right)\epsilon\ [-5.15422, 0.101203]},\quad (43)$$

$$\theta = 0.9996123 - 0.0043383\left(Log\left(\frac{P}{P^{\circ}}\right) - Log\left(\frac{KP^{\circ}}{916313.5}\right)\right) - 0.008662\left(Log\left(\frac{P}{P^{\circ}}\right) - Log\left(\frac{KP^{\circ}}{916313.5}\right)\right)^{2} - 0.0042707\left(Log\left(\frac{P}{P^{\circ}}\right) - Log\left(\frac{KP^{\circ}}{916313.5}\right)\right)^{3} - 0.0011727\left(Log\left(\frac{P}{P^{\circ}}\right) - Log\left(\frac{KP^{\circ}}{916313.5}\right)\right)^{4} - 2.80549x10^{-5}\left(Log\left(\frac{P}{P^{\circ}}\right) - Log\left(\frac{KP^{\circ}}{916313.5}\right)\right)^{5}$$

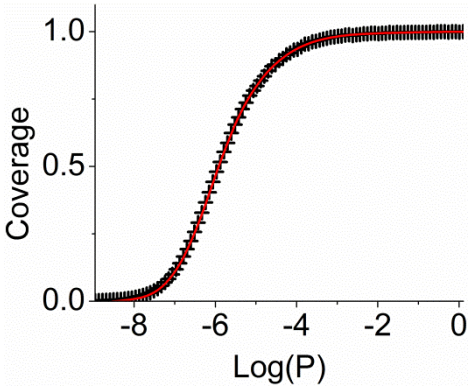

FIG. 10. Functional dependence (red line) of pressure on coverage from KMC simulations (black symbols) of dissociative adsorption on the fluorite (111) surface, fitted with a piecewise function.

The functional dependence of the log of pressure on coverage is described by piecewise fitting describing four regions (fit to KMC data shown in Figure 11):

$$\boldsymbol{For\ \theta\ \epsilon\ [0.023, 0.127875]},\quad (44)$$

$$Log\left(\frac{P}{P^{\circ}}\right) = (-5.35059 + 0.961118 * Ln(\theta)) - Log\left(\frac{KP^{\circ}}{916313.5}\right)$$

$$\boldsymbol{For\ \theta\ \epsilon\ [0.127875, 0.795813]},\quad (45)$$

$$Log\left(\frac{P}{P^{\circ}}\right) = (-8.3184 + 9.11649\theta - 11.4801\theta^{2} + 7.58151\theta^{3}) - Log\left(\frac{KP^{\circ}}{916313.5}\right)$$

$$\boldsymbol{For\ \theta\ \epsilon\ [0.795813, 0.9757]},\quad (46)$$

$$Log(\frac{P}{P^{\circ}}) = (-192.777 + 664.601\theta - 787.854\theta^2 + 314.101\theta^3) - Log(\frac{KP^{\circ}}{916313.5})$$

$$For\ \theta\ \epsilon\ [0.9757, 0.996], \quad Log(\frac{P}{P^{\circ}}) = (24106.6 - 73723.9\theta + 75100.5\theta^2 - 25484.6\theta^3) - Log(\frac{KP^{\circ}}{916313.5}) \tag{47}$$

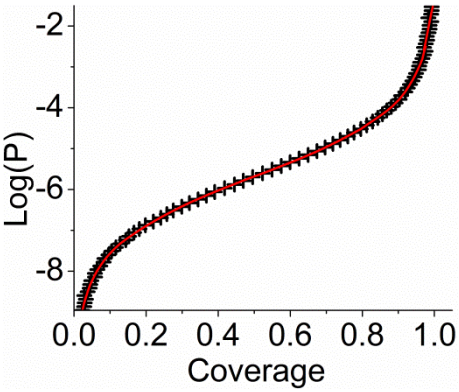

FIG. 11. Functional dependence (red line) of pressure on coverage from KMC simulations (black symbols) of dissociative adsorption on the fluorite (111) surface, fitted with a piecewise function.

Again the shift along the log(P) axis can be utilized to determine all adsorption isotherms for dissociative adsorption on the Fluorite (111) surface geometry.

IV. Discussion

By fitting to data obtained from KMC simulations, functional forms for the isotherms have been calculated for the coverage as a function of the log of pressure and the log of pressure as a function of coverage for molecular and dissociative adsorption processes on two distinct surface geometries. The functional form is general, where all adsorption isotherms can be determined by a horizontal shift of $c = \frac{W_2}{W_1}$ along the log(P) axis as shown for the analytical solutions in Section 2.2. Interestingly, it was found, for both geometries and adsorption processes, that there was no cutoff coverage for this surface (i.e. that the coverage always reached 100 percent). In previous adsorption studies involving a second order dissociative molecular adsorption process on equal sites, it was found that there was a maximum coverage that the surface would reach that was close to 90 percent coverage [1, 40].

In Figure 12 the KMC isotherms versus the analytical approximations in Eqs. 7 and 10 have been plotted. These plots give insights into what governs the functional forms of the isotherms, and similar qualitative behavior is observed for both surface geometries. At very low

coverages (i.e. $\Theta < 0.01$), there is nearly perfect agreement between the KMC simulations and the analytical solution. This shows that at very low coverages, the approximation that the "adjacent anion sites" are always unoccupied is sufficiently accurate. For low coverages (i.e. $0.01 < \Theta < 0.1$), the KMC data for both non-dissociative and dissociative adsorption processes begin to deviate from the analytical solutions. The deviation for the case of dissociative adsorption is more extreme and results from an increasing concentration of isolated dissociated species occupying the surface: these are cases where an isolated M^+ species is left behind after the M^- species originally associated with it combines with a different M^+ and leaves behind the original M^+ as the remnant. Such isolated dissociated species have a longer residence time while they wait to find a new partner for leaving, and thus lead to an underestimation of the coverage from Eqs. 7 and 10. From low to high coverage (i.e. $\Theta > 0.1$), the KMC data for molecular adsorption falls between the analytical solutions from Eq. 7 and 10: this is because in molecular adsorption, the filling of sites is correlated such that the odds of finding an open B site adjacent to an open A site are higher than the odds implied by Eq. 10. In contrast, for coverages greater than ~0.25 on both surface geometries, the KMC data for dissociative adsorption falls below both Eqs. 7 and 10. This results from an increased accumulation of dissociated species. As the concentration of dissociated species increases, the surface contains an increasing number of isolated sites associated with isolated species -- and paired sites are necessary for adsorption to occur, causing the analytical solutions to overestimate the coverage. Ultimately, we find that the KMC simulations for the non-dissociative adsorption cases are fairly well described by Eq. 10, though the piecewise fitting from this work is more accurate than Eq. 10. We find that the dissociative adsorption cases deviate significantly from both analytical solutions, and are thus only well described by the piecewise fitting from this work.

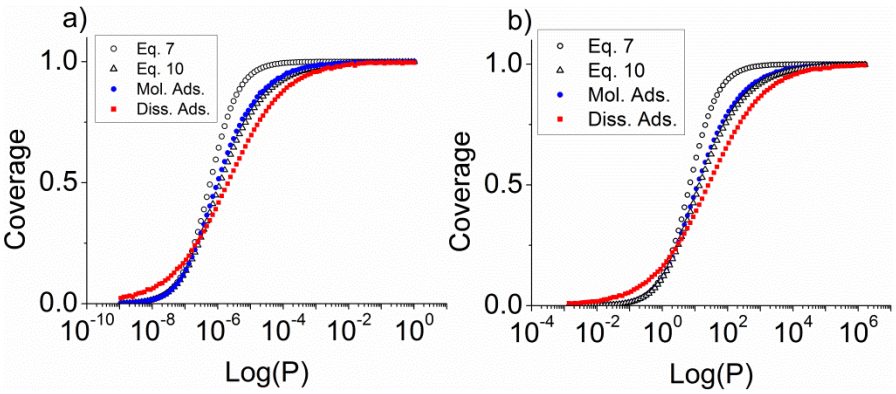

FIG. 12. Comparison of KMC adsorption isotherms to analytical solutions in Equations 7 and 10 for a) the Fluorite structure $KP^\circ = 916313.5$ and b) the perovskite structure for $KP^\circ = 0.072004$.

The KMC simulations that have been performed in the current study do not consider any coverage dependence (or molecular interactions) for adsorption, however, the same functional forms used here can be used when a coverage dependence is involved simply by using a coverage dependent equilibrium constant (i.e. $K(\Theta)$). Thus, the equations in this work can be used for cases

with molecular interactions when their interactions can be described as a function of coverage. If a coverage dependent K is being considered, it is recommended to use the piecewise fits which have been solved for the log of pressure (e.g., Eqs 44-47) since in this case an explicit function is formed, with all terms depending on Θ appearing on the right side of the equation. Whereas, using the piecewise fits which have been solved for the coverage (e.g., Eqs. 42-43) in the context of a coverage dependent rate constant results in an implicit function which is harder to solve.

During our study, we found that the functional forms which were solved for coverage (e.g., Eqs. 42-43) were prone to numerical errors when using arbitrary values of K: this was due to machine rounding errors arising from the K terms with exponents of degree >1 (such numerical errors are more likely when using a program such as Excel rather than a program with less rounding, such as Mathematica). The functional forms solved for the log of pressure (e.g., 44-47) avoid such numerical errors, since in these expressions the K terms do not have any exponents of degree >1.

V. Conclusions

Generalized functional forms for adsorption isotherms have been obtained from fitting KMC simulated data for polar non-dissociative adsorption as well as polar dissociative adsorption processes on the perovskite (100) surface and fluorite (111) surface using KMC simulations. The results for the perovskite (100) surface are also applicable to cases with the NaCl (100) structure, since the geometry is the same. The functional forms provided give accurate values for the coverage as a function of pressure, or pressure as a function of coverage. In addition, they are applicable for any values of the equilibrium constant, and can even be used in cases where the equilibrium constant varies as a function of coverage, i.e. $K(\Theta)$. Thus, the equations in this work can be used for cases with molecular interactions when their interactions can be described as a function of coverage. The functional forms which have been solved for the log of pressure (e.g., Eqs. 42-43) are less prone to numerical errors when using arbitrary values of K, and are also easier to solve when using a coverage dependent K.

Supplementary Material

See supplementary material for the complete data tables, obtained from KMC simulations, used to obtain the adsorption isotherm functional forms.

Acknowledgments

Research sponsored by the Laboratory Directed Research and Development Program of Oak Ridge National Laboratory, managed by UT-Battelle, LLC, for the U. S. Department of Energy.

References

[1] R. I. Masel, *Principles of adsorption and reaction on solid surfaces* (Wiley, New York :, 1996), Wiley series in chemical engineering; Wiley series in chemical engineering.

[2] W. Band, The Journal of Chemical Physics **8**, 178 (1940).

[3] J. Cortes G., The Journal of Chemical Physics **71**, 1038 (1979).

[4] D. N. Misra, The Journal of Chemical Physics **52**, 5499 (1970).

[5] H. D. Hurwitz, The Journal of Chemical Physics **48**, 1541 (1968).

[6] L. Tonks, The Journal of Chemical Physics **8**, 477 (1940).

[7] C. V. Heer, The Journal of Chemical Physics **55**, 4066 (1971).

[8] T. Keii, The Journal of Chemical Physics **25**, 1283 (1956).

[9] G. W. Woodbury, The Journal of Chemical Physics **77**, 6184 (1982).

[10] F. Fang, and I. Szleifer, The Journal of Chemical Physics **119**, 1053 (2003).

[11] C. A. J. Hoeve, The Journal of Chemical Physics **44**, 1505 (1966).

[12] G. Jura, and W. D. Harkins, The Journal of Chemical Physics **11**, 430 (1943).

[13] G. L. Aranovich, J. S. Erickson, and M. D. Donohue, The Journal of Chemical Physics **120**, 5208 (2004).

[14] R. Gordon, The Journal of Chemical Physics **48**, 1408 (1968).

[15] K. G. Ayappa, C. R. Kamala, and T. A. Abinandanan, The Journal of Chemical Physics **110**, 8714 (1999).

[16] B. L. Severson, and R. Q. Snurr, The Journal of Chemical Physics **126**, 134708 (2007).

[17] L. H. Taylor, W. W. Longley, and P. J. Bryant, The Journal of Chemical Physics **43**, 1184 (1965).

[18] Y. Zhan, W. L. Mattice, and D. H. Napper, The Journal of Chemical Physics **98**, 7502 (1993).

[19] A. Martinez, M. Castro, C. McCabe, and A. Gil-Villegas, The Journal of Chemical Physics **126**, 074707 (2007).

[20] F. Moulin, S. Picaud, P. N. M. Hoang, and P. Jedlovszky, The Journal of Chemical Physics **127**, 164719 (2007).

[21] J. A. Boscoboinik, S. J. Manzi, and V. D. Pereyra, Physica A: Statistical Mechanics and its Applications **389**, 1317 (2010).

[22] G. Pilania, P. X. Gao, and R. Ramprasad, The Journal of Physical Chemistry C **116**, 26349 (2012).

[23] A. Farkas, F. Hess, and H. Over, The Journal of Physical Chemistry C **116**, 581 (2012).

[24] E. Hansen, and M. Neurock, Journal of Catalysis **196**, 241 (2000).

[25] E. W. Hansen, and M. Neurock, Journal of Catalysis **196**, 241 (2000).

[26] S. Matera, H. Meskine, and K. Reuter, J Chem Phys **134**, 064713 (2011).

[27] M. Stamatakis, and D. G. Vlachos, ACS Catalysis **2**, 2648 (2012).

[28] J. K. Roberts, and A. R. Miller, Mathematical Proceedings of the Cambridge Philosophical Society **35**, 293 (1939).

[29] J. K. Roberts, Proceedings of the Royal Society of London. Series A, Mathematical and Physical Sciences **152**, 464 (1935).

[30] R. S. Nord, and J. W. Evans, The Journal of Chemical Physics **82**, 2795 (1985).

[31] K. J. Vette, T. W. Orent, D. K. Hoffman, and R. S. Hansen, The Journal of Chemical Physics **60**, 4854 (1974).

[32] A. J. Ramirez-Pastor, M. S. Nazzarro, J. L. Riccardo, and G. Zgrablich, Surface Science **341**, 249 (1995).

[33] A. J. Ramirez-Pastor, J. L. Riccardo, and V. D. Pereyra, Surface Science **411**, 294 (1998).

[34] R. Belardinelli, S. Manzi, A. J. Ramirez-Pastor, and V. D. Pereyra, Surface Science **540**, 207 (2003).

[35] J. I. Steinfeld, J. S. Francisco, and W. L. Hase, *Chemical Kinetics and Dynamics* (Prentice Hall, 1999).

[36] M. J. Hoffmann, S. Matera, and K. Reuter, Computer Physics Communications **185**, 2138 (2014).

[37] A. Savara, The Journal of Physical Chemistry C **117**, 15710 (2013).

[38] A. Savara, C. M. Schmidt, F. M. Geiger, and E. Weitz, The Journal of Physical Chemistry C **113**, 2806 (2009).

[39] T. Danielson, C. Hin, and A. Savara, (2016).

[40] H. A. Bethe, Proceedings of the Royal Society of London. Series A, Mathematical and Physical Sciences **150**, 552 (1935).